The EMBO Journal (2007) 26, 301–312 | © 2007 European Molecular Biology Organization | All Rights Reserved 0261-4189/07
www.embojournal.org

THE EMBO JOURNAL

Caenorhabditis elegans SAND-1 is essential for RAB-7 function in endosomal traffic

Dmitry Poteryaev[1], Hanna Fares[2], Bruce Bowerman[3] and Anne Spang[1,*]

[1]Biozentrum, University of Basel, Klingelbergstrasse, Basel, Switzerland, [2]Department of Molecular and Cellular Biology, University of Arizona, Tucson, AZ, USA and [3]Institute of Molecular Biology, University of Oregon, Eugene, OR, USA

The small rab-GTPase RAB-7 acts in endosome and endosome to lysosome traffic. We identified SAND-1 as a protein required for RAB-7 function based on similarities between SAND-1 and RAB-7 RNAi phenotypes. Although the initial uptake of yolk protein in oocytes, or of soluble secreted (ss) GFP in coelomocytes, appeared normal, further transport along the endocytic traffic route was delayed in the absence of SAND-1 function, and yolk proteins failed to reach yolk granules efficiently. Moreover, in coelomocytes, ssGFP and BSA-Texas-Red were endocytosed but not transported to lysosomes. We show that SAND-1 is essential for RAB-7 function at the transition from early to late endosomes, but not for RAB-7 function at lysosomes.

The EMBO Journal (2007) **26,** 301–312. doi:10.1038/sj.emboj.7601498; Published online 4 January 2007
Subject Categories: membranes & transport
Keywords: *C. elegans*; early to late endosome transport; endosomes; RAB7; RAB GTPases

Introduction

Rab proteins are regulators of membrane traffic and constitute the largest family of small GTPases with more than 60 members in mammals, about 30 in *Caenorhabditis elegans* and about 10 in *Saccharomyces cerevisiae*. Rab proteins are molecular switches. In the activated state, they are thought to recruit tethering and docking factors to the membranes to establish a firm contact between membranes destined to fuse (Pfeffer, 1999). More recently, a role for Rab proteins in cargo sorting and vesicle budding has been proposed (Morsomme and Riezman, 2002; Alvarez *et al*, 2003).

Similar to other small GTPases, Rab activity is controlled by specific nucleotide exchange factors (GEFs) and GTPase-activating proteins. Additional regulators such as GDP dissociation inhibitors (GDI) and Rab escort proteins (REPs) appear to be specific for Rab proteins, but multiple Rabs share the same GDI or REP. GDIs bind with high affinity to Rab-GDP proteins, suggesting that a GDI displacement factor (GDF) might be required to remove it so as to permit activation by a GEF (Soldati *et al*, 1994; Dirac-Svejstrup *et al*, 1997). GDFs were recently identified in yeast and humans (Yang *et al*, 1998; Sivars *et al*, 2003).

In addition to these rather common regulators, Rab proteins have multiple effectors that are usually unrelated to one another (Pfeffer, 2001; Zerial and McBride, 2001). This diversity might reflect the complex functions of Rab proteins, some of which act at multiple steps in the vesicle traffic system of the cell. For example, Rab7 acts in early to late endosome as well as in late endosome to lysosome transport (Chavrier *et al*, 1990; Feng *et al*, 1995; Meresse *et al*, 1995; Papini *et al*, 1997; Vitelli *et al*, 1997; Press *et al*, 1998). Several other Rab proteins have been localized uniquely to the early and recycling endosome compartment, where they supposedly mark different endosomal domains (Pfeffer and Aivazian, 2004), whereas late endosomes and lysosomes are marked mostly by Rab7 alone.

In mammalian cells, two effectors for Rab7 have been identified: Rab7-interacting lysosomal protein (RILP) and Rabring7 (Cantalupo *et al*, 2001; Mizuno *et al*, 2003). Both require Rab7 function for their recruitment to late endosomal and lysosomal membranes, and therefore they are likely downstream targets of Rab7. RILP has been reported to recruit a dynein–dynactin motor to the late endosomes and lysosomes and by this means promote transport of these organelles to the perinuclear region (Jordens *et al*, 2001).

Much more is known about the yeast Rab7, Ypt7p. Ypt7p is required for all membrane fusion steps where the vacuole (the yeast lysosome) is involved: autophagy, homotypic vacuolar and vesicle fusion (Haas *et al*, 1995; Lazar *et al*, 1997). For vacuolar fusion, Ypt7p interacts with a tethering complex—the HOPS complex—and a complex consisting of Ccz1p and Mon1p, which is required for SNARE pair association (Wang *et al*, 2002, 2003). At the vacuole, Ypt7p probably displaces negative regulators of membrane fusion, like the LMA1 complex, from the SNAREs before fusion (Gerst, 1999). No role for Ypt7p in early to late endosome transport has been established in yeast.

Here, we describe our identification and characterization of SAND-1, an evolutionarily conserved protein essential for RAB-7 function at early and late endosomes but not at lysosomes. This is the first characterization of a metazoan member of the SAND family. Reducing either *sand-1* or *rab-7* function resulted in a very similar phenotype, namely the accumulation of giant early and late endosomes owing to a traffic defect between the early and late endocytic compartments. Surprisingly, although knock-down of RAB-5 did not phenocopy the *sand-1* mutation, both RAB-7 and RAB-5 were more abundant in *sand-1*(*or552)* than in wild-type. In contrast, Ypt7p levels were not increased in a Δ*mon1* strain, indicating that, although conserved, the cellular environments where SAND-1 and Mon1p act might be different. Our results demonstrate that SAND-1 is required for RAB-7 function at the early and late endosomes.

*Corresponding author. Department of Biochemistry, Biozentrum, University of Basel, Klingelbergstrasse 70, 4056 Basel, Switzerland.
Tel.: +41 61 267 2380; Fax: +41 61 267 2148;
E-mail: anne.spang@unibas.ch

Received: 7 June 2006; accepted: 16 November 2006; published online: 4 January 2007

Results

or552 is a loss-of-function mutant in the C. elegans SAND family protein

or552 is a temperature-sensitive embryonic-lethal *C. elegans* mutant that accumulates large vesicle-like structures, or granules, in oocytes and embryonic cells (Poteryaev and Spang, 2005). These granules were more prominent in the anterior cell (AB cell) of two-cell stage embryos (Figure 1A). Large granules were also present at the permissive temperature, despite a decreased penetrance in embryonic lethality. Although a few of the embryos produced at 25°C hatched, these all died as young larvae (data not shown). In addition, most animals displayed severe postembryonic defects at the permissive temperature that included being dumpy and sluggish, and having other defects in body morphology (Supplementary Figure S2). Surviving adult mutant animals grown at the permissive temperature displayed abnormal large granules in coelomocytes (Poteryaev and Spang, 2005). Coelomocytes are scavenger cells that are highly active in endocytosis, and function similarly to mammalian macrophages by continuously taking up fluid from the body cavity (Fares and Greenwald, 2001a). Oocytes are also very active in endocytosis (Grant and Hirsh, 1999). The similar mutant defects observed in these two cell types suggest that the *or552* mutation affects endocytosis, directly or indirectly.

or552 is a recessive mutation with temperature-sensitive embryonic and larval lethality. The embryonic lethality at the permissive and at the restrictive temperature varied between 30–50 and 89–99%, respectively. *or552/+* heterozygote animals displayed no postembryonic morphological defects and had viable brood size undistinguishable from the wild type. When *or552* hermaphrodites were crossed with wild-type males, the cross-fertilized embryos still contained large granules, indicating a maternal requirement for this locus. However, at the same time, hatching and survival rates increased dramatically, demonstrating a role for zygotic expression from the wild-type *or552* locus. We conclude that the *or552* locus exhibits both maternal and zygotic gene expression requirements.

We cloned the *or552* mutation using a combination of three factor mapping and SNP analysis. The gene F41H10.11 contains a C to T transition at position 937 of the coding frame that results in a premature STOP codon (Supplementary Figure S1B). To further test if the premature STOP in F41H10.11 is responsible for the phenotype, we first reduced the function of F41H10.11 using RNAi. Like the *or552* mutation, RNAi-mediated knock-down of F41H10.11 caused large granules to accumulate early in embryonic development, followed by embryonic lethality and postembryonic defects in body morphogenesis and locomotion (Figure 1C and data not shown). Furthermore, recently a knockout in F41H10.11 became available, which showed an indistinguishable phenotype from the knock-down and the *or552* allele (Supplementary Figure S1D and E). We next raised polyclonal antibodies against F41H10.11 and

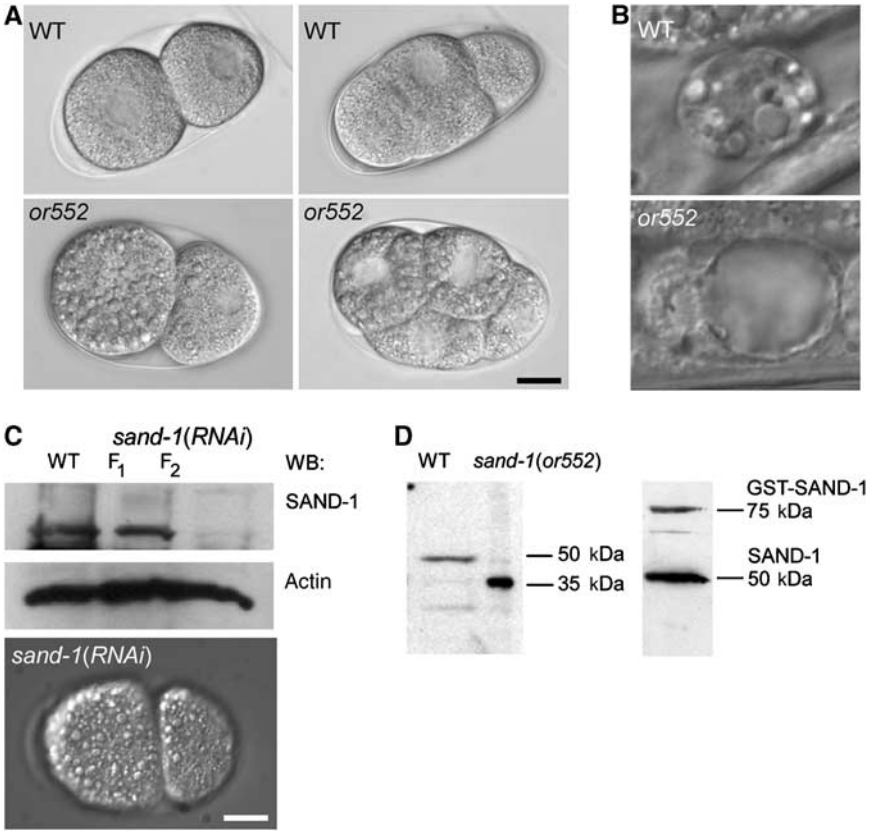

Figure 1 Phenotype and molecular identity of the *or552* mutation. (**A**) Nomarski images of wild-type and *or552* early embryos. Note the presence of large intracellular granules in *or552*. (**B**) Coelomocyte morphology by DIC in wild-type and *or552* adult worms. (**C**) RNAi of *sand-1* produced the same phenotype as the *or552* mutant. The efficiency of the knock-down was confirmed by immunoblot. Actin served as a loading control. (**D**) Immunoblot analysis of SAND-1 in wild-type and *or552* mutants. The right panel shows the immunoblot with recombinant SAND-1. The bars in panels A–C correspond to 10 μm.

determined the amount of F41H10.11 before and after dsRNA treatment (Figure 1C). The RNAi knock-down caused penetrant phenotypes in the F_2 generation, after feeding or injection of dsRNA, suggesting that either F41H10.11 is a very stable protein or the dsRNA treatment was not very effective. Finally, we prepared lysates from wild-type and *or552* mutant worms and subjected them to immunoblot analysis. A band of about 50 kDa was detected in the wild-type lysate and was absent in the *or552* lysate (Figure 1D). Instead, a 35 kDa band appeared in the *or552* lysate, which is the size predicted by the premature STOP. We conclude that the mutation in F41H10.11 is responsible for the defects observed in *or552* mutants and that the truncated F41H10.11 protein is expressed and stable in the cell.

To provide further proof for the molecular identity of *or552*, we constructed a translation fusion of F41H10.11 to GFP and generated an extrachromosomal array in *or552* worms. Unfortunately, as observed by many others, gene silencing occurred in the germ line, preventing expression of the transgene in early embryos. However, the embryonic lethality was largely rescued, indicating that zygotic expression of the fusion protein was sufficient for rescue. We were also able to detect rescue in coelomocytes. In mosaic animals, the coelomocytes that were negative for GFP::F41H10.11 maintained the large granules, whereas they were of normal size in coelomocytes that expressed the GFP::F41H10.11 fusion protein (Supplementary Figure S1C). Therefore, we are confident that the premature STOP mutation in F41H10.11 is responsible for the accumulation of large cytoplasmic granules and the lethality of the *or552* mutants.

F41H10.11 belongs to the SAND family and was named SAND-1 in accordance with *C. elegans* nomenclature. SAND family proteins are conserved from yeast to plants and mammals (Supplementary Figure S3), but only the yeast protein, Mon1p, has been characterized (Wang *et al*, 2002). The N-terminal half of SAND-1 was predicted to be structurally similar to the yeast protein Ccz1p and members of the TRAPPII complex, which is a tethering complex at the Golgi (Soding *et al*, 2005). In addition, SAND-1 contains a cyclin kinase recognition site, class III PDZ domain-binding motifs and an SH2 domain-binding motif, which are conserved between the *C. elegans* and the human proteins. However, the domain structure is unique and therefore the SAND proteins represent a novel, highly conserved protein family.

The yeast protein Mon1p forms a complex with Ccz1p, which seems to link the HOPS complex to the Rab protein Ypt7p and plays a role in the fusion of membrane structures with the vacuole (Wang *et al*, 2003). As for many other proteins involved in transport to the vacuole, Mon1p is not essential under normal growth conditions. However, the transport of the vacuolar carboxypeptidase Y (CPY) from the endosome to the vacuole is blocked, whereas the alternative alkaline phosphatase pathway remains largely unperturbed. Expression of *C. elegans* SAND-1 in a *MON1* deletion strain partially rescued the maturation of CPY (Poteryaev and Spang, 2005). Thus, SAND family members are conserved in function from yeast to worms. Finally, we performed a two-hybrid analysis and found that, similar to the yeast proteins, SAND-1 and the *C. elegans* homolog of Ccz1p can form a complex (Supplementary Table S1). We conclude that SAND-1 is the functional ortholog of yeast Mon1p.

The granules in sand-1(or552) are of endocytic origin and accumulate yolk protein

If SAND-1 acts similarly to Mon1p at the lysosome—the equivalent of the yeast vacuole—transport to the lysosome should be blocked and endosomes should accumulate, whereas early steps of endocytosis should be unaffected. First, we examined early endocytic events. We stained embryos with the lipophilic dye FM4-64, a marker of the endocytic pathway. In wild-type embryos, the plasma membrane was stained and an intracellular haze was observed, reflecting the presence of endosomes and lysosomes at this magnification (Figure 2A). In contrast, FM4-64 accumulated in the large granular structures in *sand-1*(*or552*) embryos, indicating that the uptake of FM4-64 was not disturbed and that endosomal/lysosomal trafficking was abnormal. To provide additional evidence that the initial steps of receptor-mediated endocytosis were normal, we crossed a fusion of yolk protein to GFP (VIT-2::GFP) with the *sand-1*(*or552*) mutant. As expected, receptor-mediated endocytosis of VIT-2::GFP appeared normal in *sand-1*(*or552*) oocytes and inevitably the yolk protein accumulated in large, peripheral granules (Figure 2B). Thus, the absence of SAND-1 leads to late defects in the endocytic pathway after normal internalization of membrane and solutes.

Next, we concentrated on the other end of this endocytic route, the lysosome. Surprisingly, lysosome biogenesis and size were unaffected in *sand-1*(*or552*) mutants (Figure 2C and D). This conclusion followed from (i) immunofluorescent visualization of the lysosome-specific RAB-GTPase GLO-1 (Hermann *et al*, 2005), which is expressed in intestinal cells; (ii) the appearance of autofluorescent gut granules; (iii) LysoTracker staining to mark acidic compartments, all of which appeared normal in *sand-1*(*or552*). In addition, the lysosomes were also acidified based on their staining by acridine orange (data not shown). Because lysosomes appear mostly normal in *sand-1* mutants, we infer that the wild-type gene product acts at earlier steps in endosome traffic, and that SAND-1 inactivation causing lethality in spite of the presence of lysosomes was presumably generated from other sources. One prediction based on this hypothesis is that knock-down of the lysosomal-tethering complex HOPS, which is required for all lysosomes, should result in defects different from those caused by inactivating SAND-1, and this was indeed what we found (Table I and Supplementary Figure S4). None of the characteristic defects of the *sand-1*(−) were observed upon knock-down of VPS-16 or VPS-41 or in the *vps-16*(*ok719*) mutant (Supplementary Figure S4). In contrast, in *vps-16*(*ok719*) worms, the number of autofluorescent gut granules was severely reduced (Supplementary Figure S4; Hermann *et al*, 2005). Thus, loss of SAND-1 function results in perturbations along the endocytic route upstream of the lysosomes. But which step was disturbed by the lack of SAND-1 function?

RAB-7 depletion results in accumulation of yolk protein in large granules

The enlarged yolk granules in *sand-1*(*or552*) embryos were apparent in the oocytes (Supplementary Figure S5A). When we examined the *sand-1*(*or552*) and the *sand-1*(*RNAi*) phenotypes in the gonad, we realized that the effects looked strikingly similar to ones resulting from the depletion of RAB-7 (Grant and Hirsh, 1999), suggesting that these proteins

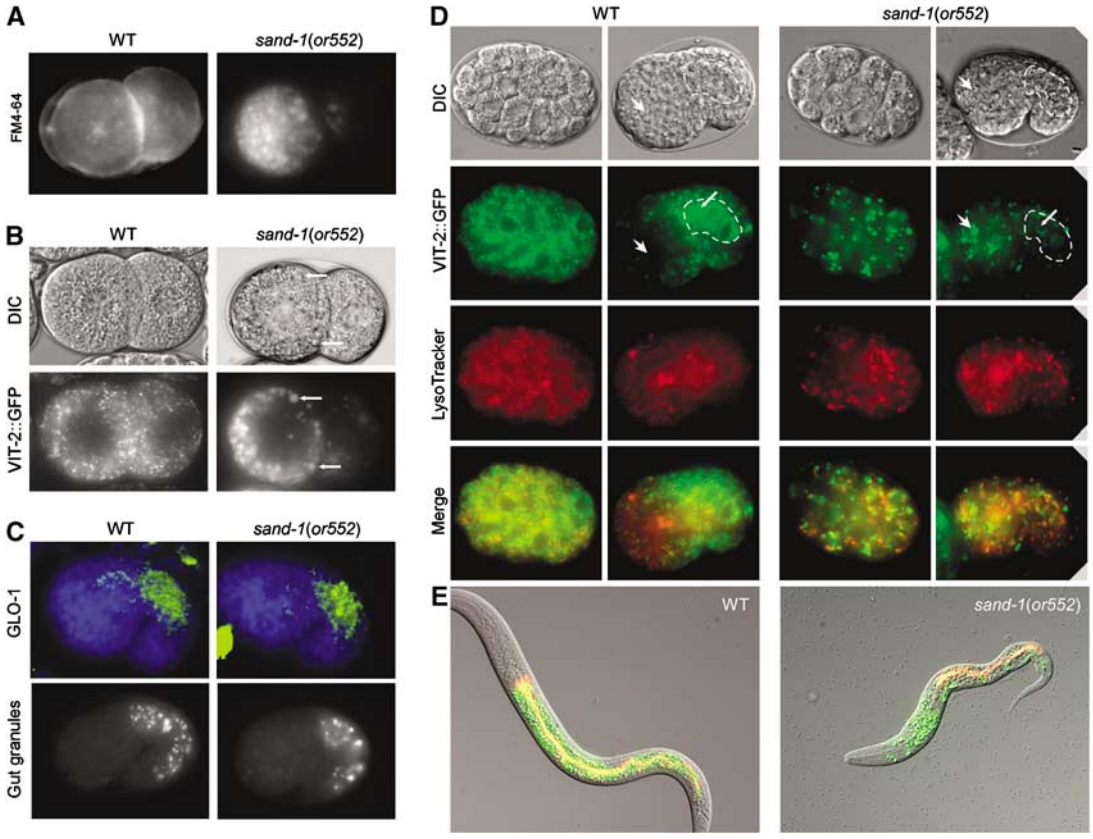

Figure 2 Yolk protein accumulates in large granules in *sand-1*(*or552*) embryo and is trapped in this compartment. (**A**) The abnormal granules in *sand-1*(*or552*) mutant embryos are of endocytic origin. FM4-64 stains enlarged granules in *sand-1* two-cell-stage mutants. The focal plane is on top of the blastomers in the case of *sand-1*(*or552*). (**B**) Enlarged granules in *sand-1*(*or552*) mutants contain yolk protein. Arrows indicate the overlap between the characteristic DIC structures and VIT-2::GFP signal. (A, B) The FM4-64-positive, VIT-2::GFP-containing granules are asymmetrically and peripherally localized in *sand-1*(*or552*) mutants. (**C**) Lysosome biogenesis appears to be unaffected in *sand-1* mutants. Upper panel: GLO-1 immunostaining of the lysosomes in the embryonic gut primordium. Nuclei are stained with DAPI. Lower panel: autofluorescent granules in the gut primordium. (**D**) LysoTracker staining and yolk protein distribution in early- and middle-stage embryos. The absence of yolk protein redistribution from the embryonic anterior region to the gut primordium (outlined) indicates incompetence of the yolk granules of regulated re-secretion in *sand-1* mutants. (**E**) Merge of DIC, LysoTracker, and VIT-2::GFP. In a wild-type larva, all the remaining yolk is found in the gut, together with gut cell lysosomes. In contrast, in a *sand-1*(*or552*) mutant larva, yolk is still trapped in the large granules randomly scattered through the body. No or little yolk reaches the gut.

Table I Epistatic interactions of *sand-1* and various endocytic effectors

Mutation	Yolk granules appearance	Yolk granules appearance in *sand-1(or552)* background	Other phenotypes
sand-1(*or552*)	Enlarged, ectopically localized	—	Emb, Lva, Bmd, Mlt, Dpy
rme-2(*RNAi*)	Rme	Rme, reduced size	Ste, Emb
chc-1(*RNAi*)	Rme	Rme, reduced size	Emb
rab-7(*RNAi*)	Enlarged, ectopically localized	Unchanged	Emb, Lva, Bmd, Mlt, Dpy
rab-5(*RNAi*)	Rme	Rme, reduced size	Emb
rab-11(*RNAi*)	Rme	Rme, reduced size	Emb
nmy-2(*RNAi*)	ND	Still peripheral but anterior-posterior asymmetry eliminated	Emb
cup-4(*ar465*)	Normal	Unchanged	Cup (also eliminates large endocytic vacuoles in *sand-1*(*or552*)
pep-5 /R06F6.2(*RNAi*)	Normal		Emb, Bmd, Lvl
vps-16(*RNAi*)	Normal		Emb
vps-41(*RNAi*)	Normal		Lva

Rme phenotype: receptor-mediated endocytosis defective (no or very little VIT-2::GFP signal in oocytes/embryos); Cup phenotype: abnormal endocytosis by coelomocytes.
Emb: embryonic lethality; Lva: larval lethality; Bmd: body morphology defects; Dpy: dumpy; Mlt: molting defects; Ste: sterile.

act in the same pathway. We tested this hypothesis by comparing the other phenotypes of *sand-1*(*or552*) with the ones due to *rab-7*(*RNAi*). Remarkably, the asymmetric distribution of the yolk granules after fertilization and the defect in efficient re-secretion and re-uptake of yolk (as scored by the failure of yolk redistribution from the anterior of the embryo to the gut primordium, and the presence of yolk protein-containing granules in the head of L1 larva) looked conspicuously similar (Figure 3B and C). The anterior enrichment of yolk protein in the early embryo presumably reflects the anterior enrichment of microfilaments observed in early *C. elegans* embryos (Strome, 1986; Munro *et al*, 2004) as microfilaments are known to be required for endocytosis. Although the peripheral distribution of the large granules was still observed after knock-down of the non-muscle myosin NMY-2, the asymmetric polarization of the oocytes and the asymmetric distribution of the yolk-containing granules were lost (data not shown).

None of the *sand-1* mutant phenotypes were observed after knock-down of the yolk protein receptor RME-2, the early endosome-associated RAB-5, recycling endosome-located RAB-11, or clathrin heavy chain (data not shown). We are confident that the knock-downs were efficient, because RNAi of RAB-5 and RAB-11 each caused embryonic lethality, defects in cytokinesis and the accumulation of multinucleated cells, phenotypes that have been reported previously (Grant and Hirsh, 1999). Finally, when we used RNAi to deplete RAB-7 in *sand-1*(*or552*) mutants, large granules remained in oocytes and embryos, whereas depletion of RAB-5 and RAB-11 caused disappearance of the large granules (Supplementary Figure S6), suggesting that they act upstream of SAND-1. In addition, *rab-7*(*RNAi*) oocytes and *sand-1*(*or552*) oocytes partially accumulated VIT-2::GFP in RME-2-positive compartments, whereas no such accumulation was ever observed in wild-type or in *vps-16*(*ok719*) (Supplementary Figure S7; Grant and Hirsh, 1999). In addition, acidification of lysosomal compartments in coelomocytes was normal both in the RAB-7 knockout strain *rab-7*(*ok511*) and in *sand-1*(*or552*) (Supplementary Figure S8A). Finally, BSA coupled to Texas Red (BSA-TR) injected into the body cavity of adult worms did not reach the lysosomes efficiently in coelomocytes in both mutants (Supplementary Figure S8B). Because depletion of RAB-7 or SAND-1 results in identical or nearly identical defects, we conclude that they may be required for the same molecular process.

The membrane association of RAB-7 is impaired in sand-1(or552)

Because knockdown of RAB-7 phenocopied *sand-1*(−), we wanted to determine whether the localization of RAB-7 on endosomes was dependent on functional SAND-1. We raised peptide antibodies against RAB-7, RAB-5, and RAB-11 (Supplementary Figure S9) and performed immunofluorescence on oocytes (Figure 4A). In wild-type oocytes, RAB-7 appeared to be mostly membrane associated. However, the *sand-1* mutation had a dramatic effect on the RAB-7 localization as it became mostly cytoplasmic and was no longer found in association with any particular structure in the cell. Furthermore, the RAB-7 signal in the mutant was much stronger than in wild-type. This effect was specific, because the membrane association of RAB-5 and RAB-11 was not affected in *sand-1*(*or552*) mutants (Figure 4A). We conclude

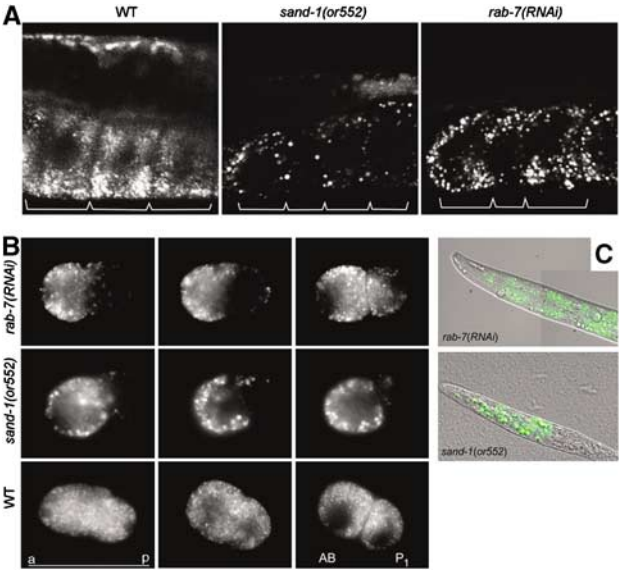

Figure 3 RNAi of *RAB-7* phenocopies the *sand-1*(*or552*) mutation. (**A**) Large VIT-2::GFP-containing granules accumulate in oocytes depleted of RAB-7. Confocal microscopy of the oocytes containing VIT-2::GFP. The borders of the oocytes are indicated with brackets. (**B**) The VIT-2::GFP granules are asymmetrically distributed upon fertilization. Shown are time-lapse frames; from left to right: fertilized egg with pseudocleavage, P_0 mitosis, two-cell stage. Note that in *rab-7*(*RNAi*) and *sand-1*(*or552*), yolk granules are mostly at the periphery of the blastomers and concentrated at the anterior pole of the P_0 cell. After the first cleavage, the AB cell receives more yolk protein than the P_1 cell. (**C**) *rab-7*(*RNAi*) larvae contain yolk granules randomly scattered through the body, similarly to *sand-1*(*or552*) larvae.

that SAND-1 is required for the membrane recruitment of RAB-7.

To confirm and to extend the results we observed in oocytes, we turned to coelomocytes, which exhibit strong morphological defects in *sand-1*(*or552*) mutants (Figure 1B). We expressed RAB-7 and RAB-5 GFP fusion proteins in coelomocytes, in both wild-type and in *sand-1*(*or552*) worms (Figure 4B). GFP::RAB-5 was membrane associated in both wild-type and mutant coelomocytes, whereas the endosome localization of GFP::RAB-7 was strongly impaired in the *sand-1*(*or552*) mutants. However, we also observed conspicuous accumulations of RAB-7 signal in granules and again it appeared as though there might be more RAB-7 present in the mutant than in the wild-type.

RAB-5 and RAB-7 are more abundant in sand-1(or552) than in wild-type

To further investigate whether SAND-1 affects the levels of RAB-7, we compared the relative amounts and the membrane association of RAB-5, RAB-7, and RAB-11 by immunoblot (Figure 4C). As expected, comparable amounts of RAB-11 were detected in wild-type and *sand-1*(*or552*), whereas a dramatic increase of RAB-7 and, unexpectedly, of RAB-5 was observed in the mutant (Figure 4C). Furthermore, as expected, the ratio of membrane-associated to soluble RAB-7 was dramatically decreased in *sand-1*(*or552*), which was not the case for the other two Rab proteins (Figure 4C). To further examine the distribution of Rab proteins in *sand-1*(−) mutants, we next loaded worm lysates on sucrose density gradients. RAB-5, RAB-7, and RAB-11 were endosome-associated

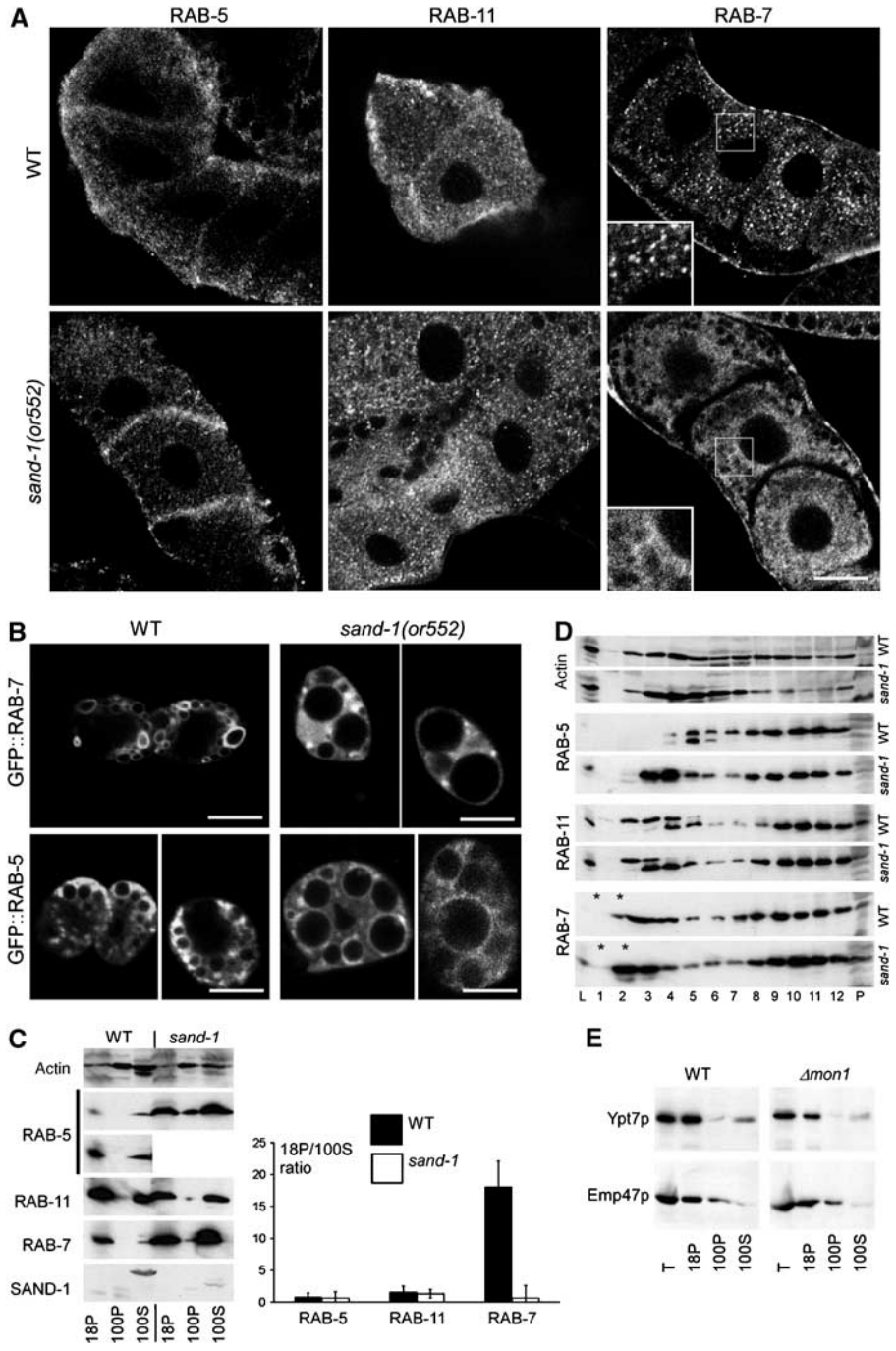

Figure 4 The effect of SAND-1 loss of function on RAB-5, RAB-7, and RAB-11 in oocytes and coelomocytes. (**A**) Immunofluorescence confocal microscopy of RAB-7, RAB-11, and RAB-5 in oocytes. RAB-7 staining shows a punctate pattern in the wild-type, whereas RAB-7 appears to be cytoplasmic and not associated with any particular structures in *sand-1*(*or552*) mutant oocytes. SAND-1 loss of function has no pronounced effect on localization of either RAB-5 or RAB-11. (**B**) Visualization of GFP::RAB-7 and GFP::RAB-5 in coelomocytes. In *sand-1*(*or552*), coelomocytes GFP::RAB-7 appear more cytoplasmic, whereas GFP::RAB-5 is still membrane bound. Scale bars in (A) and (B), 10 μm. (**C**) The ratio of membrane-bound to cytoplasmic RAB-7 is decreased in *sand-1*(*or552*). Post-nuclear lysates were subjected to centrifugation at 18 000 *g* for 20 min and then for 2 h at 100 000 *g*. 18P and 100P correspond to the pellets after the 18 000 and 100 000 *g* spins, respectively. 100S is the supernatant after the 100 000 *g* centrifugation. In the case of RAB-5, the lower panel shows a longer exposure of the wild-type material. The ratio of the signal of the RABs in the 18 000 *g* pellet and 100 000 *g* supernatant was determined by densitometry. The standard deviation of three independent experiments is given. (**D**) Analysis of RAB-5, RAB-11, and RAB-7 localization by sucrose density centrifugation. A post-nuclear supernatant from wild-type or *sand-1*(*or552*) was loaded on top of a 10–40% continuous sucrose gradient. After centrifugation, fractions were collected from the top and analyzed by SDS–PAGE and by immunoblot. Fractions are numbered according to increasing sucrose density. L is 1% of the loaded material. P is a pellet at the bottom of the gradient. The asterisks indicate the load. (**E**) Ypt7p levels are not increased in Δ*mon1* cells. A differential centrifugation was performed as above from wild-type and Δ*mon1* yeast lysate. The samples were analyzed by immunoblot with antibodies against the RAB-7 ortholog Ypt7p and the membrane protein Emp47p. Emp47p served as a loading control.

in both wild-type and mutant and migrated toward the bottom fractions, similar to what has been described previously for mammalian cells (Stockinger *et al*, 2002). However, a large portion of RAB-5 in *sand-1*(*or552*) mutant extract entered the gradient (Figure 4D, fractions 3–5; for quantification, see Supplementary Figure S10), consistent with it being associated with small vesicles or part of a large protein complex. In contrast, a considerable amount of RAB-7 in *sand-1*(*or552*) mutant extract did not enter the gradient in the mutant (Figure 4D, fraction 2; Supplementary Figure S10), indicating that this fraction of RAB-7 was cytoplasmic. Our results suggest that SAND-1 has at least two distinct functions: it recruits RAB-7 onto endosomes, and it regulates, directly or indirectly, the cellular levels of both RAB-5 and RAB-7.

The levels of RAB-7 and RAB-5 were dramatically elevated upon loss of SAND-1 function. We tested if Ypt7p and Ypt51 levels were also increased in Δ*mon1* mutants. However, this was not the case (compare Figure 4E to C and D; and data not shown), reinforcing that SAND-1 and Mon1p, despite being orthologs, act differently on RAB-7/Ypt7p.

SAND-1 localizes mostly to the cytoplasm and is peripherally membrane associated

If SAND-1 acts upstream of RAB-7, then SAND-1 localization in the cell should be unaffected by the loss of RAB-7. First, we determined the subcellular localization of SAND-1 by differential centrifugation and found that SAND-1 was exclusively cytoplasmic (Figure 4C). This result was confirmed by detecting SAND-1 in the gonad and by expressing SAND-1::GFP in coelomocytes (Figure 5A and Supplementary Figure S5B). This fusion protein is functional, as it rescued the *sand-1*(*or552*) phenotype in coelomocytes (Supplementary Figure S1). However, we also detected some membrane-associated SAND-1 in oocytes and coelomocytes. A portion of SAND-1 might be loosely associated with membranes and would be lost during worm lysis and centrifugation. The localization of the mutated SAND-1 in *or552* mutants was similar to wild-type, indicating that the premature STOP codon in *sand-1*(*or552*) does not lead to mislocalization of the presumably truncated protein. Finally, we asked whether RAB-7 influences SAND-1 localization. RNAi depletion of RAB-7 or using a maternal lethal RAB-7 knockout did not detectably alter the SAND-1 localization in oocytes (Supplementary Figure S5B and data not shown). Thus, SAND-1 is required for the membrane association of RAB-7, but RAB-7 does not appear to influence SAND-1 localization. Taken together, our results suggest that SAND-1 acts either upstream of RAB-7 to recruit RAB-7 to membranes or as a downstream tether factor.

The large granules in sand-1(or552) represent different endocytic compartments

As reported above, RAB-5 was not only found on early endosomes in wild-type coelomocytes but also was localized to some of the large granules in *sand-1*(*or552*) mutant coelomocytes, indicating that at least a subpopulation of these granules might be early endosomes (Figure 4B). To

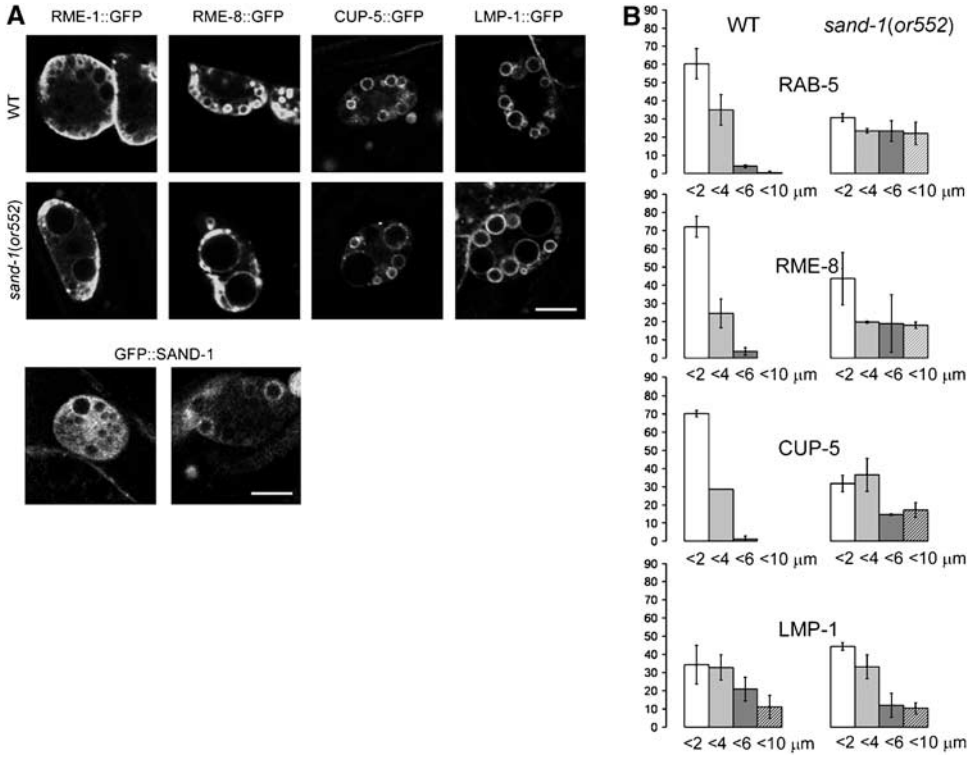

Figure 5 (**A**) Localization of different endocytic compartmental markers in wild-type and *sand-1*(*or552*) mutant coelomocytes. Worms were grown to young adults at 20°C and shifted to 25°C 4–5 h before the experiment. RME-1::GFP marks recycling endosomes, RME-8::GFP is associated with early and late endosomes, and CUP-5::GFP and LMP-1::GFP staining represent mostly lysosomes. Localization of GFP::SAND-1 in wild-type coelomocytes. The bar represents 5 μm. (**B**) Quantification of the size of endosomes and lysosomes in wild-type and *sand-1*(*or552*) coelomocytes. Organelles, which were positive for the indicated marker, were sorted into four size categories according to their diameter: 1–2, 2–4, 4–6, and 6–10 μm. Error bars represent the standard deviation.

further investigate the identity of the large granules, we used GFP fusions to markers for different endosomal compartments. First, we used a GFP fusion to the endosomal protein RME-8 (Zhang *et al*, 2001). Similar to RAB-5, considerable amounts of RME-8::GFP were associated with large granules in *sand-1*(*or552*) coelomocytes (Figure 5). Thus, some of the large granules are definitely of early endocytic origin. Next, we checked RME-1, which is an EH-domain-containing ATPase associated with recycling endosomes (Grant *et al*, 2001). In coelomocytes, RME-1 was mostly found in structures in close proximity to the plasma membrane, and their localization did not change significantly in *sand-1*(*or552*) mutants (Figure 5). Therefore, the large vacuoles do not include recycling endosomes, which might still be functional in *sand-1*(*or552*) mutants. We also checked CUP-5, which is a putative calcium channel involved in sorting from the late endosome to the lysosome (Hersh *et al*, 2002). A subpopulation of CUP-5 was found in large granules in *sand-1*(*or552*) coelomocytes. In contrast, a GFP fusion to LMP-1, which is the *C. elegans* homolog of the lysosomal protein LAMP1 was mostly absent from the enlarged granules (Figure 5). We conclude that large granules observed in *sand-1*(*or552*) mutants contain early and late endosomal and little if any lysosomal proteins. However, all of the markers always localized only to a subpopulation of the granules, indicating that the granules do not represent large conglomerates of mixed identity, but rather a mixed population of enlarged early and late endosomes that maintain distinct identities. Because two distinct classes of large granules accumulate in *sand-1* mutants, we conclude that SAND-1 is required for endocytic traffic at two stages, early to late endosomes and late endosome to lysosome. The presence of both granule classes further suggests that either the first block is incomplete or late endosomes can be produced from another source, like through the fusion of vesicles from the TGN.

Loss of SAND-1 leads to a block in early to late endosome traffic

To corroborate the result that SAND-1 is required for early to late endosomal traffic, we performed *in vivo* pulse-chase analysis of endocytosis in coelomocytes using previously established assays (Zhang *et al*, 2001; Sato *et al*, 2005). For this purpose, we expressed soluble secreted (ss) GFP from a heat-shock-inducible promoter (Fares and Greenwald, 2001b) and followed its uptake and degradation in the lysosomes over time. Three and a half hours after heat shock, the body cavity was filled with ssGFP. In addition, ssGFP accumulated in endocytic compartments in wild-type and *sand-1*(*or552*) coelomocytes, confirming again that the initial steps of endocytosis were not affected after loss of SAND-1 function (Figure 6). The body cavity of wild-type worms was cleared of ssGFP 20 h after heat shock, and some staining of endocytic structures in coelomocytes was observed. By contrast, in *sand-1*(*or552*) mutants, the body cavity was still filled with ssGFP, indicating that bulk uptake into coelomocytes was slowed down, most likely owing to the defects in early to late endosome traffic. By 27 h after heat shock, the ssGFP had all been degraded in wild-type worms, but considerable amounts of ssGFP were still present in the body cavity in the *sand-1*(*or552*) mutant, and the large granules of the coelomocytes remained filled with GFP. These results further substantiate our conclusions that traffic to the lysosomes is dramatically delayed in *sand-1*(*or552*) animals.

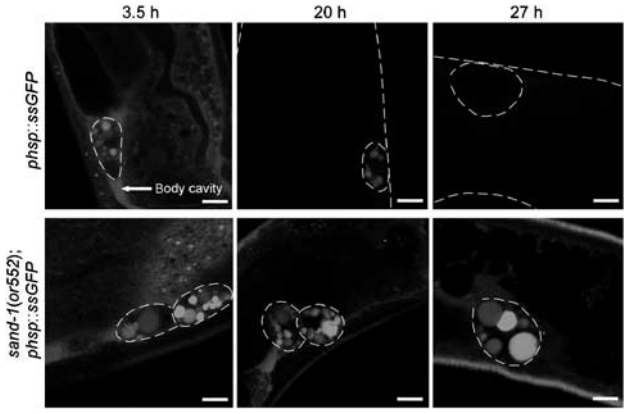

Figure 6 *sand-1*(*or552*) mutant coelomocytes are defective in the degradation of endocytosed material. Time course of ssGFP uptake and degradation by coelomocytes. The indicated times represent the time after heat-shock induction of ssGFP expression. The body wall and coelomocytes are outlined when needed to facilitate visualization. The confocal microscope image acquisition settings were the same for all images shown. The bars correspond to 5 μm.

To dissect the block in endosomal traffic with higher temporal resolution, we microinjected BSA-TR into the body cavity of adult hermaphrodites and examined the uptake of BSA-TR into the coelomocytes of worms expressing a GFP::RAB-5 fusion, which localized to early endosomes. In wild-type worms, 5 min after injection of BSA-TR into the body cavity, the marker started to accumulate in the early endosomes of the coelomocytes as indicated by the GFP-positive compartments (Figure 7A, white arrows and E). A significant amount of BSA-TR had left the GFP::RAB-5 compartment 20 min after the pulse; after 60 min, most of the BSA-TR was present in a RAB-5-negative later endocytic compartment. Again, the initial uptake of protein was normal in *sand-1*(*or552*) (Figure 7B, arrows and E). However, the BSA-TR accumulated in the early endosomes, as indicated by GFP::RAB-5 staining, and stayed there throughout the time course of the experiment. No or very little BSA-TR exited the early endosome, indicating that loss of SAND-1 function severely delays early to late endosome traffic.

Our data show that in *sand-1*(*or552*) mutants, the individual endosomes are enlarged and that the large granules do not arise by mixing of early and late endosomal compartments. This model predicts that after injection of BSA-TR into the body cavity of *sand-1*(*or552*) worms expressing LMP-1::GFP, no BSA-TR should reach the LMP-1::GFP-positive granules. This is indeed what we observed (Figure 7, compare C to D). In wild-type worms, a considerable amount of TR-BSA reached the LMP-1::GFP-positive compartment within 20 min after injection, whereas only a few of the LMP-1::GFP endosomes or lysosomes contained any TR-BSA in *sand-1*(*or552*) coelomocytes, even after 60 min. Therefore, SAND-1 is not involved in maintaining endosome integrity, but rather is required for the communication between different endosomal structures. We would predict that in the RAB-7 knockout worms, BSA-TR should not leave the GFP::RAB-5-positive compartments; this was indeed what we observed (Figure 7F). In addition, LMP-1::GFP also accumulated in early endosomes (Figure 7G),

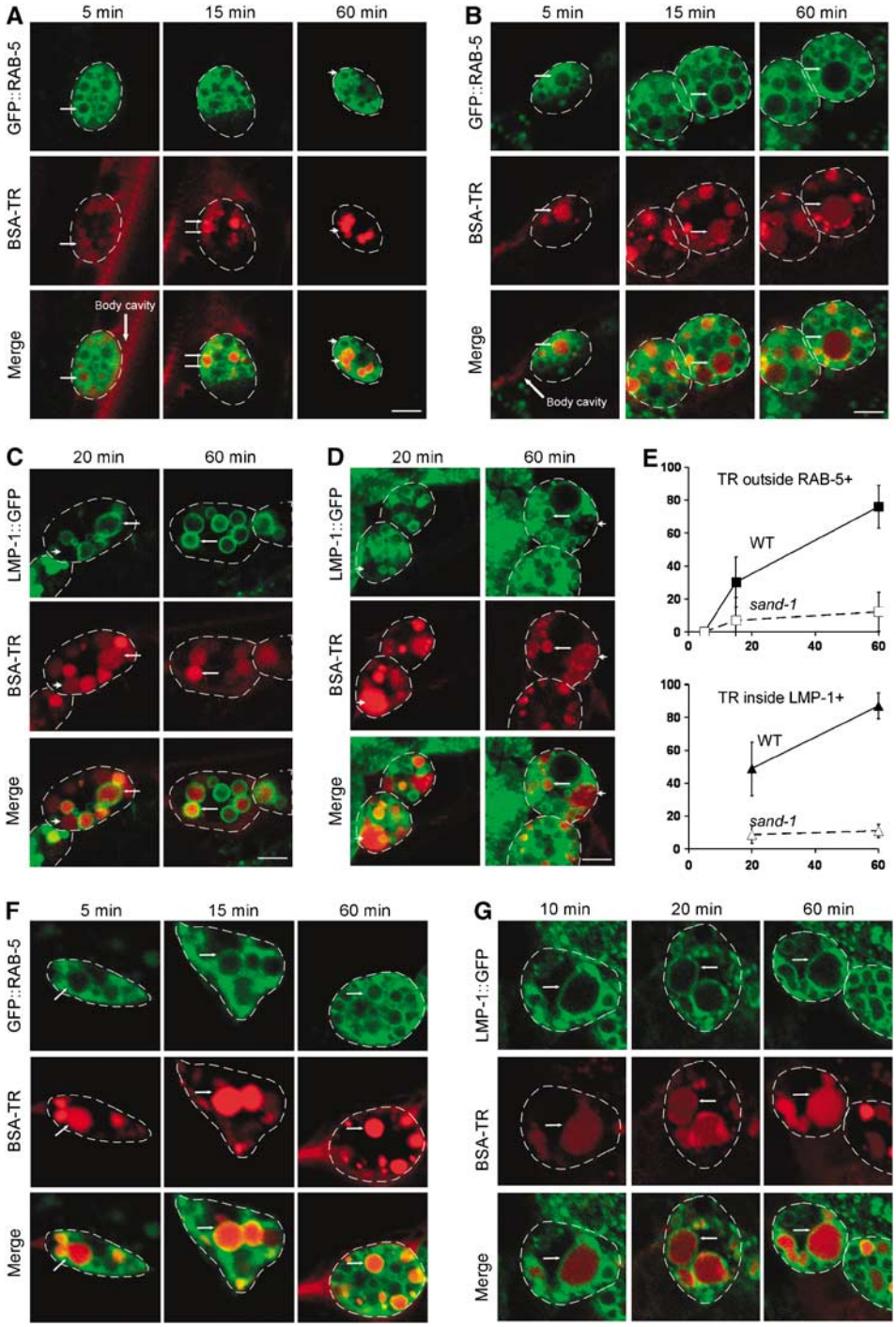

Figure 7 Endocytic traffic in *sand-1*(*or552*) mutant coelomocytes is blocked *en route* from early endosomes to late endosomes/lysosomes. Internalization of BSA-TR and its transport through endocytic compartments is shown over time after BSA-TR injection into the body cavity. Worms were grown to young adults at 20°C and shifted to 25°C 4–5 h before the experiment. (**A**) Five minutes after injection of BSA-TR, BSA-TR appears within GFP::RAB-5-positive early endosomes in wild-type and *sand-1* mutant coelomocytes (small arrows). After 15 min, BSA-TR is concentrating at the sites of exit from early endosomes, both in wild-type and *sand-1* mutants. After 60 min, most of the BSA-TR left already the GFP::RAB-5-positive early endosomal compartment in the wild-type (compare arrowheads). (**B**) *sand-1*(*or552*) mutant coelomocytes still retain BSA-TR within early endosomes (small arrows) even after 60 min of injection. (**C**) In the wild-type, after 20 min of injection, some of the BSA-TR has already reached the LMP-1::GFP-positive lysosomal/late endosomal compartment (small arrows). A portion of BSA-TR remains in the earlier LMP-1::GFP-negative pool. By 60 min, BSA-TR is concentrated in LMP-1::GFP-positive lysosomes (small arrows). (**D**) After 20 and 60 min post BSA-TR injection, most of the BSA-TR has still not reached LMP-1::GFP-positive lysosomes in *sand-1*(*or552*) mutant coelomocytes (arrowheads). A rare LMP-1::GFP-positive compartment containing BSA-TR is indicated by an arrow. The large arrows point to the body cavity where the BSA-TR was injected. Coelomocytes are outlined for better visibility. The bars in (A)–(D) correspond to 10 μm. (**E**) Quantification of the BSA-TR transport over time in wild-type and mutant coelomocytes. The percentage's of TR-positive but GFP::RAB-5-negative compartments or TR-positive and GFP::LMP-1-positive compartments with respect to the total number of TR-positive structures were scored. The error bars represent the standard deviation. The *X*-axis gives the time in minutes after the pulse. (**F**) *rab-7* deletion allele (*ok511*) shows a block of exit of BSA-TR from the GFP::RAB-5-positive endocytic compartment in coelomocytes. (**G**) LMP-1::GFP accumulates in early endosomes. TR accumulates early in the LMP-1::GFP-positive compartment of *rab-7*(*ok511*) coelomocytes. The magnification in (F) and (G) is the same as in (A)–(D).

indicating that in *rab-7*(−) the transport to lysosomes is also affected.

Taken together, our results demonstrate a requirement of SAND-1 for RAB-7 function at early and late endosomes. Although RAB-7 plays also a role at lysosomes, this function is independent of SAND-1.

Discussion

Rab GTPases must be temporally and spatially regulated to properly target and promote the fusion of different membrane-bound compartments. Here, we identified and characterized SAND-1, a novel regulator of RAB-7 in early to late endosome transport and which influences RAB-7 association with endosomes. In addition, SAND-1 may play a role in the maintenance of RAB-5 and RAB-7 levels but not of RAB-11 concentrations in cells.

SAND-1 is conserved throughout eukaryotes. Unicellular organisms, invertebrates, and plants have only one gene for SAND-1, whereas vertebrates have two related genes. Although SAND proteins are present in all eukaryotes, there are limits to the family ties. In yeast, Mon1p forms a complex with Ccz1p and this complex interacts with the HOPS complex and is required for the Ypt7p-dependent docking/tethering state (Wang *et al*, 2003). Yet unlike in yeast, we were unable to detect an interaction between SAND-1 and Ce-VPS-39, the GEF for RAB-7 and a member of the HOPS complex. Furthermore, we performed an RNAi analysis on the HOPS complex, which had no influence on yolk granule size and distribution. Therefore, Ce-CCZ-1 may still form a complex with SAND-1, however, they would act on early to late endosome transport rather than on fusion with the lysosome. In addition, mutations in the *C. elegans* ortholog of the $PI3,5P_2$ kinase, Fab1p, which is localized at the yeast vacuole and required for vacuole acidification, yielded extremely large lysosomes and not endosomes (Nicot *et al*, 2006). Moreover, the levels of Ypt7p and Ypt51p were identical in wild-type and Δ*mon1* strains, whereas the levels of RAB-7 and RAB-5 were strongly increased upon loss of SAND-1 function. Finally, unlike in *sand-1*(−) animals, LMP-1 transport to the lysosomes failed in *rab-7*(−) worms. These differences could be explained by additional roles of Rab7 versus Ypt7p. Mammalian Rab7 is not only required for late endosome to lysosome/vacuole traffic but also for early to late endosome transport (Vonderheit and Helenius, 2005). Most importantly, in *C. elegans*, the Rab GLO-1 acts specifically at lysosomes at least in the intestine (Hermann *et al*, 2005). In spite of these differences, we nevertheless observed partial rescue of a Δ*mon1* strain by expressing SAND-1. When expressed in yeast, perhaps the SAND-1/Ccz1p complex is targeted to the vacuole where it controls Ypt7p.

How does SAND-1 influence RAB-7 function? SAND-1 might act as a tethering factor at endosomes. The N-terminal half of SAND-1 is predicted to be structurally similar to Ccz1p and to the synbindin family, which are members of the TRAPP complex. There are two conserved TRAPP complexes that act as tethering factors at different steps in transit through the Golgi (Sacher *et al*, 1998). Recently, one of these complexes, TRAPPII, has been shown to act uptstream of the rab GTPase Ypt31p (Sciorra *et al*, 2005). Finally, the HOPS complex was suggested to load Rab7 on endosomes in a Rab5-dependent manner in mammalian cells (Rink *et al*, 2005). We did not obtain any evidence for this mechanism in *C. elegans*, because the RNAi of the HOPS complex did not lead to any transport block at the early or late endosomes as observed in *rab-7*(−) and *sand-1*(−) animals. In *C. elegans*, SAND-1 might help to recruit RAB-7 to early endosomes, thus potentiating their maturation into late endosome. We also tested the possibility of SAND-1 being a GEF for RAB-7 and thereby activating RAB-7 at the endosomes. However, no GEF activity could be detected (D Poteryaev and A Spang, unpublished results).

SAND-1 may act downstream of RAB-5, because knockdown of RAB-5 prevented the accumulation of large vesicles in *sand-1*(−) mutants, suggesting that it prevents passage of membrane traffic at an earlier step. However, RAB-5 levels increased in *sand-1*(−) mutants, suggesting that SAND-1 may feedback to influence RAB-5 function. One model is that SAND-1 displaces RAB-5 from membranes, with membrane association stabilizing and hence increasing the levels of RAB-5 in *sand-1*(−) mutants. Conversely, RAB-7 requires SAND-1 for its membrane association and would not be recruited efficiently to endosomes in *sand-1*(−) mutants. Perhaps RAB-7 levels rise to compensate for this defect. Alternatively, SAND-1 could be generally involved in the degradation of RAB proteins at early endosomes.

RAB-7 appears to have another, SAND-1-unrelated, function in the transport from the *trans*-Golgi to the lysosomes, because deletion of RAB-7 resulted in a misrouting of the lysosomal marker LMP-1 to the early endosome. Ihrke *et al* (2004) have shown that there are at least two distinct pathways by which LAMP1 can reach the lysosomes. In *sand-1*(−), one route (from the TGN) is still functional, whereas in *rab-7*(−), also the other LMP-1 traffic route is blocked. This is in agreement with our observation that SAND-1 acts at endosomes and not at lysosomes in *C. elegans*.

We propose that SAND-1, acting in part through RAB-7, is required for early to late endosome maturation and transport. Nevertheless, we observed two distinct classes of enlarged early and late endosomes in *sand-1* mutants. How are later stage vesicles produced in spite of the earlier block? It is likely that other routes are available (Supplementary Figure S11). For example, TGN pathways to both early and late endosomes exist, and our data show that early uptake and localization to early endosomes occur in the absence of SAND-1. Although recycling from the early endosome to the plasma membrane was also slightly impaired in *sand-1* mutants, loss of SAND-1 has no effect on RAB-11. Thus, we infer two requirements for SAND-1, one in early endosomes and one in late endosomes, to explain the accumulation of two distinct vesicle populations in *sand-1*(−) mutants. Although we think it is unlikely, we cannot exclude the presence of residual SAND-1 activity due to the relatively short shift to the restrictive temperature before the experiment. Nevertheless, these findings define novel requirements for a widely conserved protein that acts primarily on RAB-7 but also influences RAB-5 to mediate membrane trafficking events.

Materials and methods

Information about the strains and antibodies and parts of the experimental procedures are provided in supplementary data because of space limits.

Pulse chase

The traffic of BSA-TR in coelomocytes was monitored as described by Zhang *et al* (2001). At various times after microinjection, worms were mounted in 1% paraformaldehyde on agarose pads for confocal microscopy. For each time point, similar results were obtained with more than 10 coelomocytes of different worms. To follow the uptake and intracellular traffic of pseudocoelomic GFP by coelomocytes (secreted GFP pulse-chase), *dpy-20*(*e1282ts*) *IV; arIs36*[*phsp::ssGFP*] and *sand-1*(*or552*) *dpy-20*(*e1282ts*) *IV; arIs36*[*phsp::ssGFP*] worms were heat-shocked for 30 min at 33°C and then kept at 20°C for indicated times before observations. For live imaging, worms were immobilized by treatment with 10 mM levamisole in M9 and mounted on agarose pads.

For the quantification of endosome and lysosome sizes, discrete intracellular structures in at least 25 coelomocytes were analyzed for each marker. The diameters of these structures showing GFP signal on their membranes were distributed within four size categories: 1–2, 2–4, 4–6, and 6–10 μm.

Differential and gradient centrifugations

Wild-type and *sand-1*(*or552*) worms were synchronized and cultured on NGM plates. Mixed stage worms were washed off with M9, pelleted, and resuspended in 800 μl of lysis buffer (5 mM imidazole pH 7.4, 8.5% sucrose, and protease inhibitors). The worms were disrupted with a SilentCrusher S^{TM} (Heidolph Instruments). Carcasses and nuclei were removed by centrifugation for 5 min at 1000 *g* and 500 μl of the supernatant was loaded on top of a 4 ml 10–40% continuous sucrose gradient. Gradients were spun for 16 h at 40 000 r.p.m. in an SW60 rotor (Beckman Instruments). Fractions were collected from the top and TCA precipitated.

For differential centrifugation, 300 μl of the postnuclear lysate was spun subsequently at 18 000 *g* for 20 min and at 100 000 *g* for 2 h. Pellets and supernatants were reconstituted to the same volume in sample buffer containing 8 M urea.

Supplementary data

Supplementary data are available at *The EMBO Journal* Online (http://www.embojournal.org).

Acknowledgements

We thank B Grant, G Hermann, H-D Schmitt, B Singer-Krüger, Y Kohara, and A Coulson for providing us with worm strains, antibodies, cDNA, and cosmid clones. We are grateful to IG Macara for critical comments on the manuscript. Several of the strains used in this work were provided by the *Caenorhabditis* Genetics Center and the *C. elegans* knockout consortium. We are grateful to R Dale, S Wahl, and J Roberts for technical assistance. This work was supported by the Max Planck Society and the University of Basel. HF is supported by NIGMS grant GM65235.

References

Alvarez C, Garcia-Mata R, Brandon E, Sztul E (2003) COPI recruitment is modulated by a Rab1b-dependent mechanism. *Mol Biol Cell* **14:** 2116–2127

Cantalupo G, Alifano P, Roberti V, Bruni CB, Bucci C (2001) Rab-interacting lysosomal protein (RILP): the Rab7 effector required for transport to lysosomes. *EMBO J* **20:** 683–693

Chavrier P, Parton RG, Hauri HP, Simons K, Zerial M (1990) Localization of low molecular weight GTP binding proteins to exocytic and endocytic compartments. *Cell* **62:** 317–329

Dirac-Svejstrup AB, Sumizawa T, Pfeffer SR (1997) Identification of a GDI displacement factor that releases endosomal Rab GTPases from Rab-GDI. *EMBO J* **16:** 465–472

Fares H, Greenwald I (2001a) Genetic analysis of endocytosis in *Caenorhabditis elegans*: coelomocyte uptake defective mutants. *Genetics* **159:** 133–145

Fares H, Greenwald I (2001b) Regulation of endocytosis by CUP-5, the *Caenorhabditis elegans* mucolipin-1 homolog. *Nat Genet* **28:** 64–68

Feng Y, Press B, Wandinger-Ness A (1995) Rab 7: an important regulator of late endocytic membrane traffic. *J Cell Biol* **131:** 1435–1452

Gerst JE (1999) SNAREs and SNARE regulators in membrane fusion and exocytosis. *Cell Mol Life Sci* **55:** 707–734

Grant B, Hirsh D (1999) Receptor-mediated endocytosis in the *Caenorhabditis elegans* oocyte. *Mol Biol Cell* **10:** 4311–4326

Grant B, Zhang Y, Paupard MC, Lin SX, Hall DH, Hirsh D (2001) Evidence that RME-1, a conserved *C. elegans* EH-domain protein, functions in endocytic recycling. *Nat Cell Biol* **3:** 573–579

Haas A, Scheglmann D, Lazar T, Gallwitz D, Wickner W (1995) The GTPase Ypt7p of *Saccharomyces cerevisiae* is required on both partner vacuoles for the homotypic fusion step of vacuole inheritance. *EMBO J* **14:** 5258–5270

Hermann GJ, Schroeder LK, Hieb CA, Kershner AM, Rabbitts BM, Fonarev P, Grant BD, Priess JR (2005) Genetic analysis of lysosomal trafficking in *Caenorhabditis elegans*. *Mol Biol Cell* **16:** 3273–3288

Hersh BM, Hartwieg E, Horvitz HR (2002) The *Caenorhabditis elegans* mucolipin-like gene cup-5 is essential for viability and regulates lysosomes in multiple cell types. *Proc Natl Acad Sci USA* **99:** 4355–4360

Ihrke G, Kyttala A, Russell MR, Rous BA, Luzio JP (2004) Differential use of two AP-3-mediated pathways by lysosomal membrane proteins. *Traffic* **5:** 946–962

Jordens I, Fernandez-Borja M, Marsman M, Dusseljee S, Janssen L, Calafat J, Janssen H, Wubbolts R, Neefjes J (2001) The Rab7 effector protein RILP controls lysosomal transport by inducing the recruitment of dynein–dynactin motors. *Curr Biol* **11:** 1680–1685

Lazar T, Gotte M, Gallwitz D (1997) Vesicular transport: how many Ypt/Rab-GTPases make a eukaryotic cell? *Trends Biochem Sci* **22:** 468–472

Meresse S, Gorvel JP, Chavrier P (1995) The rab7 GTPase resides on a vesicular compartment connected to lysosomes. *J Cell Sci* **108:** 3349–3358

Mizuno K, Kitamura A, Sasaki T (2003) Rabring7, a novel Rab7 target protein with a RING finger motif. *Mol Biol Cell* **14:** 3741–3752

Morsomme P, Riezman H (2002) The Rab GTPase Ypt1p and tethering factors couple protein sorting at the ER to vesicle targeting to the Golgi apparatus. *Dev Cell* **2:** 307–317

Munro E, Nance J, Priess JR (2004) Cortical flows powered by asymmetrical contraction transport PAR proteins to establish and maintain anterior-posterior polarity in the early *C. elegans* embryo. *Dev Cell* **7:** 413–424

Nicot AS, Fares H, Payrastre B, Chisholm AD, Labouesse M, Laporte J (2006) The phosphoinositide kinase PIKfyve/Fab1p regulates terminal lysosome maturation in *Caenorhabditis elegans*. *Mol Biol Cell* **17:** 3062–3074

Papini E, Satin B, Bucci C, de Bernard M, Telford JL, Manetti R, Rappuoli R, Zerial M, Montecucco C (1997) The small GTP binding protein rab7 is essential for cellular vacuolation induced by *Helicobacter pylori* cytotoxin. *EMBO J* **16:** 15–24

Pfeffer S, Aivazian D (2004) Targeting Rab GTPases to distinct membrane compartments. *Nat Rev Mol Cell Biol* **5:** 886–896

Pfeffer SR (1999) Transport-vesicle targeting: tethers before SNAREs. *Nat Cell Biol* **1:** E17–E22

Pfeffer SR (2001) Rab GTPases: specifying and deciphering organelle identity and function. *Trends Cell Biol* **11:** 487–491

Poteryaev D, Spang A (2005) A role of SAND-family proteins in endocytosis. *Biochem Soc Trans* **33:** 606–608

Press B, Feng Y, Hoflack B, Wandinger-Ness A (1998) Mutant Rab7 causes the accumulation of cathepsin D and cation-independent mannose 6-phosphate receptor in an early endocytic compartment. *J Cell Biol* **140:** 1075–1089

Rink J, Ghigo E, Kalaidzidis Y, Zerial M (2005) Rab conversion as a mechanism of progression from early to late endosomes. *Cell* **122:** 735–749

Sacher M, Jiang Y, Barrowman J, Scarpa A, Burston J, Zhang L, Schieltz D, Yates III JR, Abeliovich H, Ferro-Novick S (1998) TRAPP, a highly conserved novel complex on the *cis*-Golgi that mediates vesicle docking and fusion. *EMBO J* **17:** 2494–2503

Sato M, Sato K, Fonarev P, Huang CJ, Liou W, Grant BD (2005) Caenorhabditis elegans RME-6 is a novel regulator of RAB-5 at the clathrin-coated pit. *Nat Cell Biol* **7:** 559–569

Sciorra VA, Audhya A, Parsons AB, Segev N, Boone C, Emr SD (2005) Synthetic genetic array analysis of the PtdIns 4-kinase Pik1p identifies components in a Golgi-specific Ypt31/rab-GTPase signaling pathway. *Mol Biol Cell* **16:** 776–793

Sivars U, Aivazian D, Pfeffer SR (2003) Yip3 catalyses the dissociation of endosomal Rab–GDI complexes. *Nature* **425:** 856–859

Soding J, Biegert A, Lupas AN (2005) The HHpred interactive server for protein homology detection and structure prediction. *Nucleic Acids Res* **33:** W244–W248

Soldati T, Shapiro AD, Svejstrup AB, Pfeffer SR (1994) Membrane targeting of the small GTPase Rab9 is accompanied by nucleotide exchange. *Nature* **369:** 76–78

Stockinger W, Sailler B, Strasser V, Recheis B, Fasching D, Kahr L, Schneider WJ, Nimpf J (2002) The PX-domain protein SNX17 interacts with members of the LDL receptor family and modulates endocytosis of the LDL receptor. *EMBO J* **21:** 4259–4267

Strome S (1986) Asymmetric movements of cytoplasmic components in *Caenorhabditis elegans* zygotes. *J Embryol Exp Morphol* **97:** 15–29

Vitelli R, Santillo M, Lattero D, Chiariello M, Bifulco M, Bruni CB, Bucci C (1997) Role of the small GTPase Rab7 in the late endocytic pathway. *J Biol Chem* **272:** 4391–4397

Vonderheit A, Helenius A (2005) Rab7 associates with early endosomes to mediate sorting and transport of Semliki forest virus to late endosomes. *PLoS Biol* **3:** e233

Wang CW, Stromhaug PE, Kauffman EJ, Weisman LS, Klionsky DJ (2003) Yeast homotypic vacuole fusion requires the Ccz1–Mon1 complex during the tethering/docking stage. *J Cell Biol* **163:** 973–985

Wang CW, Stromhaug PE, Shima J, Klionsky DJ (2002) The Ccz1–Mon1 protein complex is required for the late step of multiple vacuole delivery pathways. *J Biol Chem* **277:** 47917–47927

Yang X, Matern HT, Gallwitz D (1998) Specific binding to a novel and essential Golgi membrane protein (Yip1p) functionally links the transport GTPases Ypt1p and Ypt31p. *EMBO J* **17:** 4954–4963

Zerial M, McBride H (2001) Rab proteins as membrane organizers. *Nat Rev Mol Cell Biol* **2:** 107–117

Zhang Y, Grant B, Hirsh D (2001) RME-8, a conserved J-domain protein, is required for endocytosis in *Caenorhabditis elegans*. *Mol Biol Cell* **12:** 2011–2021